

Extended Universal Joint Source-Channel Coding for Digital Semantic Communications: Improving Channel-Adaptability

Eunsoo Kim, *Graduate Student member, IEEE*, Yoon Huh, *Graduate Student member, IEEE*, and Wan Choi, *Fellow, IEEE*

Abstract—Recent advances in deep learning (DL)-based joint source–channel coding (JSCC) have enabled efficient semantic communication in dynamic wireless environments. Among these approaches, vector quantization (VQ)-based JSCC effectively maps high-dimensional semantic feature vectors into compact codeword indices for digital modulation. However, existing methods, including universal JSCC (uJSCC), rely on fixed, modulation-specific encoders, decoders, and codebooks, limiting adaptability to fine-grained SNR variations. We propose an extended universal JSCC (euJSCC) framework that achieves SNR- and modulation-adaptive transmission within a single model. euJSCC employs a hypernetwork-based normalization layer for fine-grained feature vector normalization and a dynamic codebook generation (DCG) network that refines modulation-specific base codebooks according to block-wise SNR. To handle block fading channels, which consist of multiple coherence blocks, an inner–outer encoder-decoder architecture is adopted, where the outer encoder and decoder capture long-term channel statistics, and the inner encoder and decoder refine feature vectors to align with block-wise codebooks. A two-phase training strategy, i.e., pretraining on AWGN channels followed by finetuning on block fading channels, ensures stable convergence. Experiments on image transmission demonstrate that euJSCC consistently outperforms state-of-the-art channel-adaptive digital JSCC schemes under both block fading and AWGN channels.

Index Terms—joint source-channel coding, semantic communication, vector quantization, adaptive normalization

I. INTRODUCTION

The sixth-generation (6G) vision targets ultra-dense connectivity, near-zero latency, and high reliability, but conventional bit-level transmission is inefficient for complex task-oriented data in dynamic, bandwidth-limited environments. Semantic communication [1]–[5] therefore prioritizes task-relevant information over bit-perfect reconstruction, and deep learning (DL)-based joint source–channel coding (JSCC) enables end-to-end encoder–decoder design by mapping semantic feature vectors directly to channel symbols and performing target tasks from channel-impaired feature vectors, which removes separate source and channel codecs while improving robustness and spectral efficiency [6].

However, transmitting continuous-valued feature vectors, referred to as analog JSCC, requires analog modulation that is incompatible with modern digital infrastructures, and channel noise directly distorts feature values, potentially causing

E. Kim, Y. Huh and W. Choi are with the Department of Electrical and Computer Engineering, Seoul National University (SNU), and the Institute of New Media and Communications, SNU, Seoul 08826, Korea (e-mail: es3783, mnihy621, wanchoi@snu.ac.kr) (*Corresponding author: Wan Choi*)

unstable task performance under poor channels or multi-hop networks [7]. These drawbacks motivate digital JSCC, where feature vectors are quantized into bitstreams and transmitted via standard digital modulation (e.g., BPSK, 4QAM, 16QAM).

Existing digital JSCC methods are generally categorized into scalar quantization (SQ) and vector quantization (VQ) approaches. SQ-based digital JSCC (SQ-JSCC) discretizes feature vectors element-wise, mapping each scalar element to a learned quantization level [8] or a point in a modulation-specific constellation [9], [10]. In contrast, VQ-based JSCC (VQ-JSCC) jointly quantizes multi-dimensional feature vectors using learned codebooks, effectively capturing inter-dimensional correlations and achieving superior rate–distortion performance [11]–[14].

In practice, wireless channels are inherently time-varying due to fading, interference, and user mobility. Training and maintaining separate JSCC models for every possible channel condition would incur prohibitive memory and computational costs. Therefore, a unified JSCC model capable of adapting to diverse channel conditions is essential for practical deployment. However, existing studies [9], [11], [12] lack such adaptability, leading to severe performance degradation under unseen channel environments.

To address channel variations in SQ-JSCC, [8] proposed a framework in which the network split point is adaptively selected according to the channel conditions, and the intermediate feature vectors at the chosen depth are scalar-quantized and transmitted. Research that splits a neural network between the transmitter and receiver by considering computational constraints at the transmitter and the signal-to-noise ratio (SNR) conditions has been explored, as in [15], and the authors in [8] further posited that feature vectors produced at different network depths contain different semantic information and exhibit varying levels of noise resistance. Therefore, they proposed a learned policy-network-based method that determines the optimal split point according to the SNR values. In addition, since the distribution of feature vectors varies with network depth, the quantization levels for each split point are individually optimized. However, the encoder–decoder process itself does not adapt to the channel condition, thereby limiting overall adaptability.

Another line of research, [10] introduced a multi-order digital joint coding-modulation (MDJCM) built upon a non-linear transform coding (NTC) [16], which adjusts the length of feature vectors according to their estimated entropy. This

scheme incorporates two kinds of conditional modules which take a modulation order and SNR value as input conditions, respectively, both implemented using the squeeze-and-excitation (SE) layer [17]. Since SE layer learns to assign larger weights to more important feature vector channel dimensions, these conditional modules adaptively emphasize the magnitude of feature elements that become more informative under the given transmission conditions. However, the quantization process in MDJCM is done with 2-dimensional segments from each feature vectors, using constellation map as a 2-dimensional fixed codebook as in [9]. Although higher modulation orders reduce quantization error from finer constellations, the feature vector dimensionality does not increase with modulation orders, limiting the amount of information that can be represented. As a result, the task performance gain saturates.

On the other hand, since each *multi-dimensional* feature vector is mapped to a single codeword index in VQ-JSCC, even one bit error can corrupt the transmitted index, leading to the receiver decoding a vastly different codeword. This high sensitivity severely distorts the alignment between the extracted feature vector and the received codeword, causing substantial task performance degradation. Consequently, VQ-JSCC is inherently vulnerable to channel impairments, particularly under low-SNR or fading conditions. To enhance robustness, it is therefore essential to adapt not only the encoder-decoder process but also the codebook itself, ensuring that the alignment between feature vectors and codewords remains consistent across varying channel conditions. In other words, VQ-JSCC must be capable of channel-adaptively aligning the feature vector space with the multi-dimensional codebook to achieve optimal task performance.

To address this challenge, a feedback-driven codebook optimization (FDCO) [13] proposed adapting codewords using an SNR-conditioned multilayer perceptron (MLP) trained after pretraining the encoder, decoder, and codebook. However, this method assumes a fixed modulation scheme and independently updates each codeword via a shared MLP while freezing the encoder and decoder during adaptation. As a result, the joint alignment between features and codewords is disrupted, ultimately limiting the achievable performance of VQ-JSCC under diverse channel conditions.

Another work [14] introduced a universal JSCC (uJSCC) framework that extends VQ-JSCC to support multiple modulation orders with negligible parameter overhead. In uJSCC, modulation-specific codebooks are paired with switchable normalization layers in the encoder and decoder. Since distinct codebooks yield different feature vector statistics, uJSCC employs a dedicated normalization layer for each modulation to stabilize these statistics and ensure adaptability across modulation conditions. However, a key limitation is that the encoder, decoder, and codebooks remain fixed for a given modulation order, which is utilized within the predefined corresponding SNR range. In practice, even when the same modulation is used, different SNR values produce different error characteristics. Thus, leveraging finer channel conditions, including not only modulation order-aware adjustment but also additional adaptation to the SNR values within each modulation region, can further improve the adaptability of the

JSCC network.

To overcome these limitations, we therefore propose an *extended universal JSCC (euJSCC)*, enhancing channel adaptability of uJSCC even for time-varying channels by adapting encoder, decoder, and codebook to both discrete modulation orders and continuously varying SNR. Specifically, switchable normalization layer is extended from modulation-conditioned operation to continuous SNR-conditioned operation, enabling fine-grained normalization during encoding/decoding. Moreover, euJSCC employs dynamic codebook generation conditioned on modulation and SNR instead of fixed modulation-specific codebooks, enabling finer channel-adaptive vector quantization.

Furthermore, contrary to the assumption of static channels with constant fading and SNR per source transmission, we consider *block fading channels* of multiple coherence blocks with different SNRs, which arise in practical wireless systems, e.g., in high-mobility scenarios [18]. Inspired by the coarse-to-fine refinement principle in [19], euJSCC extends coarse-to-fine adaptation to VQ-JSCC via an inner-outer encoder-decoder architecture: the outer encoder-decoder uses long-term channel statistics and a coarse modulation order, while the inner encoder-decoder refines channel dimensions and feature vector statistics to align with generated codebooks conditioned on block-wise SNR and the selected modulation order. All components, including normalization layer, JSCC encoder-decoder and the codebook generator, are designed with parameter efficiency for scalable adaptation. We comprehensively evaluate the proposed framework under various semantic communication scenarios.

For fair comparison, we extend uJSCC [14] and MDJCM [10] to the block fading scenario and evaluate their performance alongside comprehensive ablation studies. Experimental results demonstrate that euJSCC achieves superior and more stable task performance than state-of-the-art channel-adaptive digital JSCC schemes across diverse SNR conditions and coherence block lengths.

A. Contributions

The contributions of this article are summarized as follows:

- An euJSCC framework is proposed to enable both SNR- and modulation-adaptive semantic communication within a unified model. To achieve adaptive feature vector normalization, a parameter-efficient, hypernetwork-based normalization layer is introduced, generating modulation- and SNR-dependent parameters to allow fine-grained adaptability with minimal additional overhead.
- The framework incorporates a dynamic VQ codebook generation network tailored to diverse channel conditions. Rather than fully regenerating codebooks, it efficiently refines modulation-specific base codebooks through SNR-conditioned intra- and inter-codeword adaptations.
- To enable deployment in realistic, time-varying wireless environments, in which a single source is conveyed across multiple coherence blocks, the euJSCC adopts an inner-outer encoder-decoder structure with a two-phase training strategy. In the first phase, training on AWGN

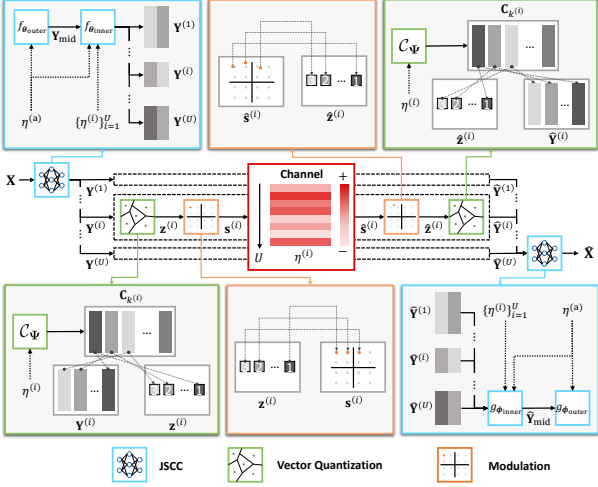


Fig. 1. System overview of euJSCC, which performs block-wise feature vector encoding-decoding, VQ, and modulation.

channels without the inner encoder–decoder establishes stable feature–codebook alignment. Subsequently, the second phase finetunes the full euJSCC model on block fading channels to ensure robustness under rapidly varying channel conditions.

- Extensive experiments under both AWGN and block fading channels demonstrate that euJSCC consistently outperforms existing channel-adaptive digital JSCC schemes in terms of reconstruction quality, robustness, and channel adaptability, while maintaining parameter efficiency across diverse datasets and channel conditions.

B. Notations

Vectors and matrices are expressed in lower case and upper case bold, respectively. $[\cdot]^{\top}$ denotes the transpose of a matrix or vector. $[\mathbf{A}]_{i,j}$, $[\mathbf{A}]_{i,:}$, and $[\mathbf{A}]_{:,j}$ represent the (i, j) -th element, the i -th row, and the j -th column of the matrix \mathbf{A} . $\mathcal{CN}(\boldsymbol{\mu}, \boldsymbol{\Sigma})$ is complex normal distribution with mean vector $\boldsymbol{\mu}$ and covariance matrix $\boldsymbol{\Sigma}$. \mathbf{I}_m is $m \times m$ identity matrix.

II. SYSTEM MODEL

A. System Preliminaries and Channel Model

Consider a point-to-point digital semantic communication system for image transmission over time-varying wireless channels. The system comprises a JSCC encoder–decoder, a vector quantizer–dequantizer, a VQ codebook generator, and a modulator–demodulator pair. We assume a block fading channel characterized by a constant coherence block length T , defined as the number of transmitted digital symbols during which the channel fading remains constant. Let N denote the total number of transmitted symbols. The transmission is divided into $U = \lceil N/T \rceil$ coherence blocks, indexed by $i \in [1:U]$. For notational simplicity, we first assume that N is an integer multiple of T , so that all U blocks have an equal length of T . However, our framework can be readily extended to the general case where N is not an integer multiple of T , as detailed in Section III-A.

Given the channel coefficient $h^{(i)}$ and the power of AWGN σ^2 , the block-wise SNR of the i -th coherence block is defined

as $\eta^{(i)} = \frac{|h^{(i)}|^2 P}{\sigma^2}$, where P denotes the average power of the transmitted digital symbols during a coherence block. The block-wise SNR $\eta^{(i)}$ is estimated at the receiver and fed back to the transmitter before the transmission of the digital symbols in each block i . We assume that the long-term channel statistics $\mathbb{E}[|h^{(i)}|^2]$ are known to both the transmitter and the receiver, and thus the average SNR, defined as $\eta^{(a)} = \frac{\mathbb{E}[|h^{(i)}|^2] P}{\sigma^2}$, is also known at both sides.

The system adaptively switches among K modulation orders such as $\{m_1, m_2, \dots, m_K\}$, where m_k represents the k -th modulation order and, without loss of generality, $m_1 < m_2 < \dots < m_K$. The modulation order for the i -th coherence block, denoted by $m_{k^{(i)}}$, is then selected according to $\eta^{(i)}$ and a predefined set of SNR boundaries $\mathbf{b} = [b_1, \dots, b_{K-1}]$ ¹:

$$m_{k^{(i)}} = \begin{cases} m_1, & \text{if } \eta^{(i)} < b_1, \\ m_k, & \text{if } b_{k-1} \leq \eta^{(i)} < b_k, \\ m_K, & \text{if } \eta^{(i)} \geq b_{K-1}, \end{cases} \quad (1)$$

where $k \in [2:K-1]$ and $k^{(i)}$ is the modulation order index for the i -th block. We assume $\eta^{(i)}$ is perfectly known at both the transmitter and receiver, ensuring synchronization of the selected modulation order.

B. euJSCC Communication Process

With the above settings, the semantic communication proceeds as follows. The end-to-end operation of the euJSCC system under block fading channels is also summarized in **Algorithm 1**.

1) Adaptive Semantic Encoding and Vector Quantization:

Given a source image $\mathbf{X} \in \mathbb{R}^{C \times H \times W}$, where C , H , and W denote the number of feature channels, height, and width, respectively, the JSCC encoder \mathcal{F}_{Θ} generates block-wise adapted feature vectors sequentially over U coherence blocks. For the i -th block, the encoder generates an adapted feature vector $\mathbf{Y}^{(i)}$ by exploiting the average SNR $\eta^{(a)}$ and the block-wise SNR $\eta^{(i)}$. Consequently, the set of block-wise feature vectors $\{\mathbf{Y}^{(i)}\}_{i=1}^U$ are produced.

To effectively respond to short-term channel fading variations, the encoder is decomposed into an outer encoder $f_{\theta_{\text{outer}}}$ and an inner encoder $f_{\theta_{\text{inner}}}$, parameterized respectively by θ_{outer} and θ_{inner} , so that $\Theta = \{\theta_{\text{outer}}, \theta_{\text{inner}}\}$. The outer encoder adapts to the long-term channel quality captured by $\eta^{(a)}$ and produces an intermediate feature vector sequence, while the inner encoder refines this sequence in a sequential block-wise manner, producing the i -th block's feature vectors conditioned on $\eta^{(a)}$ and $\eta^{(i)}$. The implementation of outer-inner encoder is provided in Section III-A.

The detailed process is as follows. The outer encoder outputs an intermediate feature vector sequence $\mathbf{Y}_{\text{mid}} = [\mathbf{y}_{\text{mid},1}, \dots, \mathbf{y}_{\text{mid},N}]^{\top} \in \mathbb{R}^{N \times D_{k^{(a)}}}$, conditioned on $\eta^{(a)}$:

$$\mathbf{Y}_{\text{mid}} = f_{\theta_{\text{outer}}}(\mathbf{X}, \eta^{(a)}), \quad (2)$$

¹Since explicitly signaling the modulation order for every transmission is infeasible, we adopt the conventional adaptive modulation and coding (AMC) strategy, where each modulation order is determined according to a predefined SNR range. The design of these SNR boundaries is discussed in Section V.

where $k^{(a)}$ is the modulation index selected by applying $\eta^{(a)}$ to the selection rule in (1), and $D_{k^{(a)}} \in \{D_1, \dots, D_K\}$ is the corresponding feature vector channel dimension. We assume $D_1 < \dots < D_K$, indicating that higher modulation orders are assigned higher-dimensional feature vectors.

The intermediate sequence is then partitioned into U non-overlapping segments of length T as $\mathbf{Y}_{\text{mid}}^{(i)} = [\mathbf{y}_{\text{mid},(i-1)T+1}, \dots, \mathbf{y}_{\text{mid},iT}]^\top \in \mathbb{R}^{T \times D_{k^{(a)}}}$ for $i \in [1:U]$. Each coherence block is then processed sequentially. For block i , $f_{\theta_{\text{inner}}}$ refines $\mathbf{Y}_{\text{mid}}^{(i)}$ into $\mathbf{Y}^{(i)} \in \mathbb{R}^{T \times D_{k^{(i)}}}$ based on $\eta^{(a)}$ and $\eta^{(i)}$:

$$\mathbf{Y}^{(i)} = f_{\theta_{\text{inner}}}(\mathbf{Y}_{\text{mid}}^{(i)}, \eta^{(a)}, \eta^{(i)}). \quad (3)$$

Here, $D_{k^{(i)}} \in \{D_1, \dots, D_K\}$ denotes the feature vector channel dimension corresponding to the modulation order index $k^{(i)}$ selected for the i -th block.

Next, for digital transmission, the extracted feature vectors $\mathbf{Y}^{(i)}$ are quantized through VQ. A dynamic codebook generator (DCG) network produces block-wise codebook $\mathbf{C}^{(i)} = [\mathbf{c}_1^{(i)}, \dots, \mathbf{c}_{m_{k^{(i)}}}^{(i)}]^\top \in \mathbb{R}^{m_{k^{(i)}} \times D_{k^{(i)}}}$ corresponding to $k^{(i)}$, conditioned on $\eta^{(i)}$. Here, $\mathbf{c}_j^{(i)} \in \mathbb{R}^{D_{k^{(i)}}}$ denotes the j -th codeword of the i -th block and the number of codewords of $\mathbf{C}^{(i)}$ is set equal to the modulation order $m_{k^{(i)}}$. Specifically, $\eta^{(i)}$ is fed into the DCG network \mathcal{C}_Ψ , parameterized by Ψ , generating the codebook as $\mathbf{C}^{(i)} = \mathcal{C}_\Psi(\eta^{(i)})$. The organization of DCG network is described in Section III-B. A quantization index of the t -th feature vector $\mathbf{y}_t^{(i)}$ is obtained as $z_t^{(i)} = \arg \min_{j \in [1:m_{k^{(i)}}]} \|\mathbf{y}_t^{(i)} - \mathbf{c}_j^{(i)}\|_2^2$ for $t \in [1:T]$. The resulting index sequence of block i is $\mathbf{z}^{(i)} = [z_1^{(i)}, z_2^{(i)}, \dots, z_T^{(i)}]^\top \in [1:m_{k^{(i)}}]^T$, which is mapped one-to-one to a modulation constellation $\mathbb{S}_{m_{k^{(i)}}} = \{s_1, \dots, s_{m_{k^{(i)}}}\} \subset \mathbb{C}$. The transmitter transmits a modulated symbol sequence $\mathbf{s}^{(i)} = [s_{z_1^{(i)}}, s_{z_2^{(i)}}, \dots, s_{z_T^{(i)}}]^\top \in \mathbb{C}^T$, normalized to satisfy the average power constraint $\mathbb{E}[\|\mathbf{s}^{(i)}\|_2^2] = P$.

2) *Wireless Channel Input-Output Relation:* The wireless channel input-output relationship of the i -th coherence block is expressed as

$$\hat{\mathbf{s}}^{(i)} = h^{(i)} \mathbf{s}^{(i)} + \mathbf{n}^{(i)}, \quad (4)$$

where $\hat{\mathbf{s}}^{(i)} = [\hat{s}_{z_1^{(i)}}, \hat{s}_{z_2^{(i)}}, \dots, \hat{s}_{z_T^{(i)}}]^\top \in \mathbb{C}^T$ denotes the received symbol vectors, and the noise vector and fading coefficient are given, respectively, as $\mathbf{n}^{(i)} \sim \mathcal{CN}(\mathbf{0}, \sigma^2 \mathbf{I}_T)$ and $h^{(i)} \sim \mathcal{CN}(0, 1)$, which remains constant within each block.

3) *Adaptive Vector Dequantization and Semantic Decoding:* Symmetrically to the transmitter, the receiver employs a JSCC decoder \mathcal{G}_Φ comprising an inner decoder $g_{\phi_{\text{inner}}}$ and an outer decoder $g_{\phi_{\text{outer}}}$, each parameterized by ϕ_{inner} and ϕ_{outer} , respectively, so that $\Phi = \{\phi_{\text{inner}}, \phi_{\text{outer}}\}$. Also, its implementation is detailed in Section III-A.

For the i -th coherence block, the receiver first performs channel equalization prior to demodulation, yielding $\tilde{\mathbf{s}}^{(i)} = \hat{\mathbf{s}}^{(i)} / h^{(i)} = \mathbf{s}^{(i)} + \mathbf{n}^{(i)} / h^{(i)}$. The symbols are then demodulated to obtain the estimated index sequence $\hat{\mathbf{z}}^{(i)} = [\hat{z}_1^{(i)}, \dots, \hat{z}_T^{(i)}]^\top \in [1:m_{k^{(i)}}]^T$. Using the same block-wise codebook $\mathbf{C}^{(i)}$, generated by \mathcal{C}_Ψ with given $\eta^{(i)}$ at the

Algorithm 1 Communication Process of euJSCC

- 1: **Input:** Source image \mathbf{X} , average SNR $\eta^{(a)}$, block-wise SNR $\{\eta^{(i)}\}_{i=1}^U$, corresponding modulation order $\{m_{k^{(i)}}\}_{i=1}^U$, coherence block length T , outer encoder-decoder $(f_{\theta_{\text{outer}}}, g_{\phi_{\text{outer}}})$, inner encoder-decoder $(f_{\theta_{\text{inner}}}, g_{\phi_{\text{inner}}})$, DCG network \mathcal{C}_Ψ
- 2: Encoder \mathbf{X} into \mathbf{Y}_{mid} with $\eta^{(a)}$ via $f_{\theta_{\text{outer}}}$
- 3: Partition \mathbf{Y}_{mid} into $\{\mathbf{Y}_{\text{mid}}^{(i)}\}_{i=1}^U$
- 4: **for** $i \leftarrow 1$ to U **do**
- 5: Adapt $\mathbf{Y}_{\text{mid}}^{(i)}$ into $\mathbf{Y}^{(i)}$ with $\eta^{(a)}$ and $\eta^{(i)}$ via $f_{\theta_{\text{inner}}}$
- 6: Generate $\mathbf{C}^{(i)}$ with $\eta^{(i)}$ via \mathcal{C}_Ψ
- 7: Quantize $\mathbf{Y}^{(i)}$ into $\mathbf{z}^{(i)}$ using $\mathbf{C}^{(i)}$
- 8: Modulate $\mathbf{z}^{(i)}$ into $\mathbf{s}^{(i)}$ via $m_{k^{(i)}}$ -ary modulation
- 9: Transmit $\mathbf{s}^{(i)}$ through block fading channel with $\eta^{(i)}$
- 10: Demodulate $\tilde{\mathbf{s}}^{(i)}$ to $\hat{\mathbf{z}}^{(i)}$ via $m_{k^{(i)}}$ -ary modulation
- 11: Dequantize $\hat{\mathbf{z}}^{(i)}$ into $\hat{\mathbf{Y}}^{(i)}$ using $\mathbf{C}^{(i)}$
- 12: Adapt $\hat{\mathbf{Y}}^{(i)}$ into $\hat{\mathbf{Y}}_{\text{mid}}^{(i)}$ with $\eta^{(a)}$ and $\eta^{(i)}$ via $g_{\phi_{\text{inner}}}$
- 13: Aggregate $\{\hat{\mathbf{Y}}_{\text{mid}}^{(i)}\}_{i=1}^U$ to reconstruct $\hat{\mathbf{Y}}_{\text{mid}}$
- 14: Reconstruct $\hat{\mathbf{X}}$ from $\hat{\mathbf{Y}}_{\text{mid}}$ with $\eta^{(a)}$ via $g_{\phi_{\text{outer}}}$
- 15: **Output:** $\hat{\mathbf{X}}$

receiver², the received feature vectors are reconstructed as $\hat{\mathbf{Y}}^{(i)} = [\mathbf{c}_{\hat{z}_1^{(i)}}^{(i)}, \dots, \mathbf{c}_{\hat{z}_T^{(i)}}^{(i)}]^\top \in \mathbb{R}^{T \times D_{k^{(i)}}}$. The demodulated and dequantized feature vectors $\hat{\mathbf{Y}}^{(i)} \in \mathbb{R}^{T \times D_{k^{(i)}}}$ are first refined by the inner decoder $g_{\phi_{\text{inner}}}$ to reconstruct intermediate feature vectors $\hat{\mathbf{Y}}_{\text{mid}}^{(i)} \in \mathbb{R}^{T \times D_{k^{(a)}}}$ conditioned on $\eta^{(a)}$ and $\eta^{(i)}$:

$$\hat{\mathbf{Y}}_{\text{mid}}^{(i)} = g_{\phi_{\text{inner}}}(\hat{\mathbf{Y}}^{(i)}, \eta^{(i)}, \eta^{(a)}). \quad (5)$$

After processing all U blocks sequentially with inner decoder, the intermediate feature vectors $\{\hat{\mathbf{Y}}_{\text{mid}}^{(i)}\}_{i=1}^U$ are concatenated to a intermediate feature vector sequence $\hat{\mathbf{Y}}_{\text{mid}} = [\hat{\mathbf{Y}}_{\text{mid}}^{(1)\top}, \dots, \hat{\mathbf{Y}}_{\text{mid}}^{(U)\top}]^\top \in \mathbb{R}^{N \times D_{k^{(a)}}}$. Finally, the outer decoder $g_{\phi_{\text{outer}}}$ reconstructs the source image $\hat{\mathbf{X}}$ from $\hat{\mathbf{Y}}_{\text{mid}}$ condition on $\eta^{(a)}$:

$$\hat{\mathbf{X}} = g_{\phi_{\text{outer}}}(\hat{\mathbf{Y}}_{\text{mid}}, \eta^{(a)}). \quad (6)$$

C. End-to-End Training Objective

To enable end-to-end training despite the non-differentiable quantization step, we adopt the VQ-VAE framework [20] with a straight-through estimator (STE). Formally, the overall training objective is defined as:

$$\begin{aligned} \mathcal{L} = \mathbb{E}_{\mathbf{X}}[\text{MSE}(\hat{\mathbf{X}}, \mathbf{X}) + \frac{1}{U} \sum_{i=1}^U \alpha_{k^{(i)}} \cdot \text{MSE}(\hat{\mathbf{Y}}^{(i)}, \mathbf{Y}_d^{(i)}) \\ + \frac{1}{U} \sum_{i=1}^U \beta_{k^{(i)}} \cdot \text{MSE}(\mathbf{Y}^{(i)}, \hat{\mathbf{Y}}_d^{(i)})], \end{aligned} \quad (7)$$

where MSE denotes the mean squared error function, and \mathbf{Y}_d is a detached copy of \mathbf{Y} used to block gradient propagation.

Given a fixed set of coefficient pairs $\{\alpha_k, \beta_k\}_{k=1}^K$, the block-wise parameters $\{(\alpha_{k^{(i)}}, \beta_{k^{(i)}})\}_{i=1}^U$ act as hyperparameters that control the relative weight of each loss component

²Since the receiver is equipped with an identical DCG network, it can generate the same codebook.

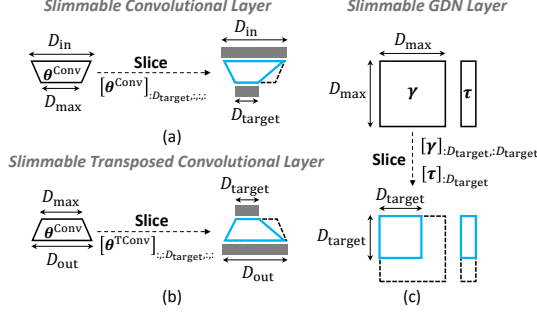


Fig. 2. An illustration of slimmable operation on (a) convolutional layer, (b) transposed convolutional layer, and (c) GDN layer.

corresponding to $k^{(i)}$. The first term represents the image reconstruction loss, ensuring pixel-level fidelity. The second term, the codebook loss, aligns the codebook embeddings with the encoder feature vectors assigned to them, while the third term, the commitment loss, constrains the encoder outputs to remain close to their corresponding codewords. Together, these two losses mitigate the mismatch between $\hat{\mathcal{Y}}$ and \mathcal{Y} , thereby enabling stable and consistent end-to-end training with the STE despite the discrete nature of the quantization step. Since the codebook loss and commitment loss largely vary with the codebook dimension D_k and codebook size m_k , different (α_k, β_k) values are applied for each modulation order.

III. EXTENDED UNIVERSAL JOINT SOURCE-CHANNEL CODING

The proposed euJSCC framework adaptively performs feature encoding/decoding and codebook generation according to the block-wise SNR $\eta^{(i)}$. This adaptive behavior is enabled by two key components: (i) an outer-inner encoder-decoder architecture designed for block fading scenarios, which parameter-efficiently processes feature vectors whose channel dimensions dynamically vary with the current channel conditions, and (ii) the DCG network, which generates codebooks tailored to block-wise SNR value and the selected modulation order. In the following, we describe these two components in detail and then introduce the hypernetwork-based normalization layer, which serves as the core mechanism for adapting feature vector distributions with respect to SNR and modulation order conditions in those two key components.

A. Implementation of the Encoder-Decoder Architecture

In block fading channels, the coherence time may be short, causing the block-wise SNR to vary significantly across blocks. To address this situation, [19] proposed a two-phase encoding-decoding process consisting of a coarse-grained phase, which uses the average SNR computed from long-term channel statistics, and a fine-grained phase, which handles rapid short-term channel fluctuations. Motivated by this idea, we integrate a similar strategy into the design of our VQ-JSCC encoder-decoder architecture for digital semantic communication, enabling robust and efficient operation under block fading channels.

The JSCC encoder \mathcal{F}_Θ and decoder \mathcal{G}_Φ , introduced in Sections II-B1 and II-B3, are implemented as stacks of (transposed) convolutional neural network (CNN) blocks. Each

block consists of a (transposed) convolutional layer followed by a (inverse) generalized divisive normalization (GDN) layer, which are widely adopted in JSCC models for its ability to capture inter-channel dependencies of the output tensor channels from each neural network (NN) layer. Additionally, both the inner encoder $f_{\theta_{\text{inner}}}$ and inner decoder $g_{\phi_{\text{inner}}}$ are implemented with parallel instances of a single convolutional layer and a (inverse) GDN layer to enable low-complexity, block-wise refinement that adapts to the instantaneous channel conditions. The standard (inverse) GDN operations are introduced in **Remark 1**.

Remark 1 (Standard GDN and inverse GDN). *Let \mathbf{t}_n denote the output tensor with D_{in} tensor channel dimensions from the n -th layer, and $t_{n,d,p}$ denote the p -th element in the d -th tensor channel of \mathbf{t}_n . The standard GDN operation produces the normalized tensor $\tilde{\mathbf{t}}_n$ as:*

$$\tilde{t}_{n,d,p} = \frac{t_{n,d,p}}{\sqrt{\tau_d + \sum_{d'=1}^{D_{\text{in}}} \gamma_{d',d} t_{n,d',p}^2}}, \quad d \in [1:D_{\text{in}}], \quad (8)$$

where $\tau \in \mathbb{R}^{D_{\text{in}}}$ is a bias vector and $\gamma \in \mathbb{R}^{D_{\text{in}} \times D_{\text{in}}}$ is a coefficient matrix. Symmetrically, the inverse GDN (IGDN) operation performs the inverse operation using its own set of parameters:

$$\tilde{t}_{n,d,p} = t_{n,d,p} \sqrt{\tau_d + \sum_{d'=1}^{D_{\text{in}}} \gamma_{d',d} t_{n,d',p}^2}, \quad d \in [1:D_{\text{in}}], \quad (9)$$

Before detailing the specific architectures for \mathcal{F}_Θ and \mathcal{G}_Φ , it is important to introduce the *slimmable operations* used to handle the varying feature vector channel dimensions $D_k \in \{D_1, \dots, D_K\}$ that arise from adapting to different modulation orders. Standard NN layers require fixed input and output tensor channel dimensions. However, in a VQ-JSCC system that should support multiple dimensions according to the current modulation order condition, maintaining separate networks for each possible input or output channel dimension significantly increases system and memory complexity. A slimmable operation [21] enables each NN layer type to reuse a single set of weights while processing or producing tensors with different channel dimensions. This mechanism is one of the key components of our parameter-efficient design, and its application to three types of NN layer utilized in \mathcal{F}_Θ and \mathcal{G}_Φ is described below.

- **Slimmable Convolutional Layer** [21]: Let $\theta^{\text{Conv}} \in \mathbb{R}^{D_{\text{max}} \times D_{\text{in}} \times \kappa \times \kappa}$ denote the weight tensor of a 2D convolutional layer with kernel size $\kappa \times \kappa$ (or $\theta^{\text{Conv}} \in \mathbb{R}^{D_{\text{max}} \times D_{\text{in}} \times \kappa}$ for the 1D case). Here, D_{in} is the input tensor channel dimension and D_{max} is the maximum output tensor channel dimension supported by the layer. In a standard convolutional layer, all D_{max} filters, the shape of which is $D_{\text{in}} \times \kappa \times \kappa$ (or $D_{\text{in}} \times \kappa$ for the 1D case), are applied to the input tensor to produce an output tensor with channel dimension D_{max} . In order to generate an output tensor with varying channel dimension D_{target} , as shown in Fig. 2(a), the same weight tensor is shared, but only the first D_{target} filters, i.e., $[\theta^{\text{Conv}}]_{:D_{\text{target}},:,:}$ (or $[\theta^{\text{Conv}}]_{:D_{\text{target}},:,:}$ for the 1D case), are used.

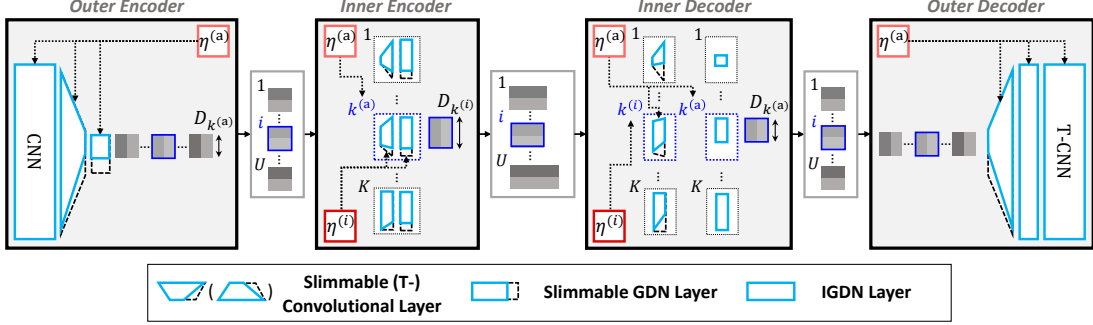


Fig. 3. The overall euJSCC encoder-decoder architecture, decomposed into inner and outer modules. "CNN", "T-CNN", and "Slimmable T-Convolutional Layer" denote CNN blocks, transposed CNN blocks, and slimmable transposed convolutional layer, respectively. The blue-highlighted path shows an example processing flow for the i -th coherence block.

- **Slimmable Transposed Convolutional Layer [21]:** Let $\theta^{\text{TConv}} \in \mathbb{R}^{D_{\text{out}} \times D_{\text{max}} \times \kappa \times \kappa}$ denote the weight tensor of a 2D transposed convolutional layer with kernel size $\kappa \times \kappa$ (or $\theta^{\text{TConv}} \in \mathbb{R}^{D_{\text{out}} \times D_{\text{max}} \times \kappa}$ for the 1D case). Here, D_{max} is the maximum input tensor channel dimension supported by the layer and D_{out} is the output tensor of channel dimension. In contrast to the convolutional layer, as shown in Fig. 2(b), when the input tensor has varying channel dimension D_{target} , the sliced weight tensor $[\theta^{\text{TConv}}]_{:,D_{\text{target}},:,:}$ (or $[\theta^{\text{TConv}}]_{:,:,D_{\text{target}},:}$ for the 1D case) is applied to the input tensor to produce an output tensor with channel dimension D_{out} .
- **Slimmable GDN Layer:** Based on the standard GDN operation defined in (8), we apply the slimmable operations to its normalization parameters. The full parameters for input tensors with channel dimension D_{max} , i.e., $\tau \in \mathbb{R}^{D_{\text{max}}}$ and $\gamma \in \mathbb{R}^{D_{\text{max}} \times D_{\text{max}}}$ are stored. Fig. 2(c) shows that when input tensor has a channel dimension $D_{\text{target}} \leq D_{\text{max}}$, the layer uses only the leading sub-vector $[\tau]_{:D_{\text{target}}}$ and the leading sub-matrix $[\gamma]_{:D_{\text{target}},:D_{\text{target}}}$ to perform the GDN operation.

Now, we describe how these slimmable operations are integrated into the specific encoder-decoder architecture. The overall process is illustrated in Fig. 3.

Outer Encoder $f_{\theta_{\text{outer}}}$: $f_{\theta_{\text{outer}}}$ generates an intermediate feature vector sequence \mathbf{Y}_{mid} (Sec. II) with channel dimension $D_{k^{(a)}} \in \{D_1, \dots, D_K\}$ determined by $\eta^{(a)}$. To support this variable-dimensional output, the final CNN block of $f_{\theta_{\text{outer}}}$ uses a single slimmable convolutional layer followed by a slimmable GDN layer.

Inner Encoder $f_{\theta_{\text{inner}}}$: The partitioned feature vectors $\mathbf{Y}_{\text{mid}}^{(i)}$ are processed by $f_{\theta_{\text{inner}}}$. $f_{\theta_{\text{inner}}}$ receives feature vectors with channel dimension $D_{k^{(a)}}$ and produces output feature vectors with channel dimension $D_{k^{(i)}} \in \{D_1, \dots, D_K\}$ determined by $\eta^{(i)}$. Therefore, the module is implemented using K parallel 1D slimmable convolutional layers followed by slimmable GDN layers. Conditioned on $\eta^{(a)}$, the $k^{(a)}$ -th layer is activated to process the input $\mathbf{Y}_{\text{mid}}^{(i)}$ with input channel dimension $D_{k^{(a)}}$, and $f_{\theta_{\text{inner}}}$ adaptively produces $\mathbf{Y}^{(i)}$ with the target dimension $D_{k^{(i)}}$ specified by $\eta^{(i)}$.

Inner Decoder $g_{\phi_{\text{inner}}}$: Symmetrically, $g_{\phi_{\text{inner}}}$ refines the received and demodulated feature vectors $\hat{\mathbf{Y}}^{(i)}$ with channel dimension $D_{k^{(i)}}$ into feature vectors with the channel dimension $D_{k^{(a)}} \in \{D_1, \dots, D_K\}$. Specifically, the module

is implemented using K parallel 1D slimmable convolutional layers followed by IGDN layers. Conditioned on $\eta^{(i)}$ and $\eta^{(a)}$, the $k^{(i)}$ -th slimmable convolutional layer and the $k^{(a)}$ -th IGDN layer are activated to process the input $\hat{\mathbf{Y}}^{(i)}$ with channel dimension $D_{k^{(i)}}$ and adaptively produce the refined output with channel dimension $D_{k^{(a)}}$.

Outer Decoder $g_{\phi_{\text{outer}}}$: After concatenating all refined block-wise feature vectors into $\hat{\mathbf{Y}}_{\text{mid}}$, $g_{\phi_{\text{outer}}}$ decodes $\hat{\mathbf{Y}}_{\text{mid}}$ to reconstruct $\hat{\mathbf{X}}$. To accommodate the variable channel dimension $D_{k^{(a)}}$, the first transposed CNN block uses a slimmable transposed convolutional layer followed by an IGDN layer.

Remark 2 (Case of $N \neq TU$): *In this case, the definitions for the final U -th block are modified accordingly. While the first $U-1$ blocks are processed as described above, the inner operations for the final block are given by:*

$$\mathbf{Y}_{\text{mid}}^{(U)} = [\mathbf{y}_{\text{mid},(U-1)T+1}, \dots, \mathbf{y}_{\text{mid},N}]^{\top} \in \mathbb{R}^{T_U \times D_{k^{(a)}}}, \quad (10)$$

$$\mathbf{Y}^{(U)} = f_{\theta_{\text{inner}}}(\mathbf{Y}_{\text{mid}}^{(U)}, \eta^{(U)}, \eta^{(a)}) \in \mathbb{R}^{T_U \times D_{k^{(U)}}}, \quad (11)$$

$$\hat{\mathbf{Y}}_{\text{mid}}^{(U)} = g_{\phi_{\text{inner}}}(\hat{\mathbf{Y}}^{(U)}, \eta^{(U)}, \eta^{(a)}) \in \mathbb{R}^{T_U \times D_{k^{(a)}}}, \quad (12)$$

where $T_U = N - (U-1)T$ is the length of the final block and $\hat{\mathbf{Y}}^{(U)} \in \mathbb{R}^{T_U \times D_{k^{(U)}}}$ is the corresponding dequantized feature vectors at the receiver. Concatenating $\{\hat{\mathbf{Y}}_{\text{mid}}^{(i)}\}_{i=1}^U$ then correctly reconstructs $\hat{\mathbf{Y}}_{\text{mid}} \in \mathbb{R}^{N \times D_{k^{(a)}}}$.

B. Dynamic Codebook Generator

In VQ-JSCC, adapting feature vectors to the wireless channel condition alone is insufficient. A proper alignment of the VQ codebook to the extracted feature vectors is also crucial. Moreover, since the optimal codebook varies with SNR, using a fixed codebook for each modulation order can lead to significant mismatches between the feature vectors produced by the JSCC encoder at the transmitter and the codewords detected at the receiver. Such mismatches degrade performance by increasing feature distortion errors.

To address these challenges, we propose the DCG network, which adaptively transforms a base codebook for each modulation order into an SNR-specific codebook. As illustrated in Fig. 4(a), the DCG network comprises three key components that operate according to the input SNR $\eta^{(i)}$ and the corresponding modulation order index $k^{(i)}$.

- 1) **Base Codebook:** For each modulation order $k^{(i)} \in [1:K]$, we employ a base codebook $\bar{\mathbf{C}}_{k^{(i)}} =$

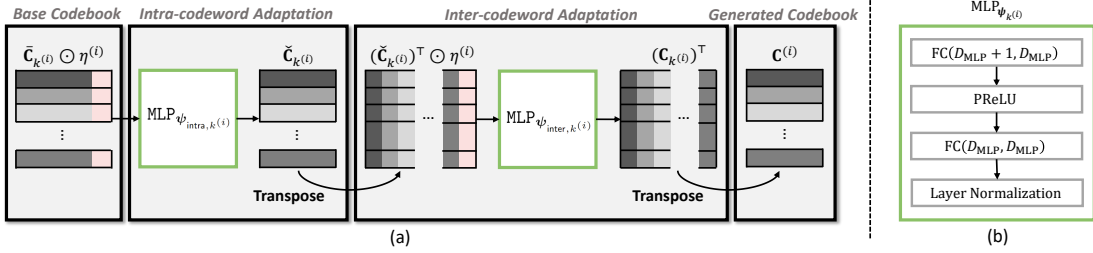


Fig. 4. An illustration of the proposed DCG network, which dynamically generates an SNR-adaptive codebook conditioned on η . For each modulation order k , a base codebook $\bar{\mathbf{C}}_k$, an intra-codeword adaptation $\text{MLP}_{\psi_{\text{intra},k^{(i)}}}$, and an inter-codeword adaptation $\text{MLP}_{\psi_{\text{inter},k^{(i)}}}$ are separately maintained, and the components corresponding to the given $k = k^{(i)}$ according to $\eta^{(i)}$ are activated. Both $\text{MLP}_{\psi_{\text{intra},k^{(i)}}}$ and $\text{MLP}_{\psi_{\text{inter},k^{(i)}}}$ follow the structure $\text{MLP}_{\psi_{k^{(i)}}}$ shown on (b), where $D_{\text{MLP}} = D_{k^{(i)}}$ and $D_{\text{MLP}} = m_{k^{(i)}}$, respectively.

$[\bar{\mathbf{c}}_{k^{(i)},1}, \dots, \bar{\mathbf{c}}_{k^{(i)},m_{k^{(i)}}}]^\top \in \mathbb{R}^{m_{k^{(i)}} \times D_{k^{(i)}}}$, where $\bar{\mathbf{c}}_{k,j} \in \mathbb{R}^{D_{k^{(i)}}}$ is the j -th base codeword for the k -th modulation order.

2) **Intra-codeword Adaptation:** Since the base codebooks are not optimal for the block-wise SNR $\eta^{(i)}$, we refine each base codeword with an SNR-conditioned transformation. Specifically, each base codeword $\bar{\mathbf{c}}_{k^{(i)},j} \in \mathbb{R}^{D_{k^{(i)}}}$ is concatenated with $\eta^{(i)}$ and passed through an intra-codeword adaptation multi-layer perceptron (MLP) $\text{MLP}_{\psi_{\text{intra},k^{(i)}}}$, parameterized by $\psi_{\text{intra},k^{(i)}}$, such as:

$$\check{\mathbf{c}}_{k^{(i)},j} = \text{MLP}_{\psi_{\text{intra},k^{(i)}}}(\bar{\mathbf{c}}_{k^{(i)},j} \odot \eta^{(i)}), \quad (13)$$

where \odot denotes the concatenation operation along the column dimensions. $\text{MLP}_{\psi_{\text{intra},k^{(i)}}}$ is composed of two fully connected layers followed by a layer normalization (LN) layer, with hidden dimension $D_{\text{MLP}} = D_{k^{(i)}}$ in Fig. 4(b). Applying this adaptation to all $m_{k^{(i)}}$ codewords yields the intra-adapted codebook $\check{\mathbf{C}}_{k^{(i)}} = [\check{\mathbf{c}}_{k^{(i)},1}, \dots, \check{\mathbf{c}}_{k^{(i)},m_{k^{(i)}}}]^\top \in \mathbb{R}^{m_{k^{(i)}} \times D_{k^{(i)}}}$.

3) **Inter-codeword Adaptation:** While intra-codeword adaptation adjusts each codeword individually, it does not consider the relative geometry among codewords. This geometric structure is particularly critical at low SNRs for each modulation, where detection errors frequently occur. If the neighboring constellation symbols are mapped to codewords that are far apart in feature space, small detection errors on the constellation map can cause large task performance degradation at the decoder. To address this, we apply inter-codeword adaptation, refining the codebook column-wise after intra-codeword adaptation. Let $[\check{\mathbf{C}}_{k^{(i)}}]_{:,d} \in \mathbb{R}^{m_{k^{(i)}}}$ denote the d -th column of the intra-adapted codebook, which collects the d -th component of a codeword across all $m_{k^{(i)}}$ codewords. Similarly, $[\check{\mathbf{C}}_{k^{(i)}}]_{:,d}$ is concatenated with $\eta^{(i)}$ and then processed by inter-codeword adaption MLP $\text{MLP}_{\psi_{\text{inter},k^{(i)}}}$, which is parameterized by $\psi_{\text{inter},k^{(i)}}$:

$$[\mathbf{C}_{k^{(i)}}]_{:,d} = \text{MLP}_{\psi_{\text{inter},k^{(i)}}}([\check{\mathbf{C}}_{k^{(i)}}]_{:,d} \odot \eta^{(i)}), \quad (14)$$

where the MLP architecture is identical to that of $\text{MLP}_{\psi_{\text{intra},k^{(i)}}}$, except that $D_{\text{MLP}} = m_{k^{(i)}}$. Stacking the outputs across all columns produces the final SNR-adaptive codebook for $m_{k^{(i)}}$, i.e., $\mathbf{C}^{(i)} \in \mathbb{R}^{m_{k^{(i)}} \times D_{k^{(i)}}}$.

The overall DCG network can be viewed as a unified network \mathcal{C}_{Ψ} , parameterized by $\Psi = \{\psi_{\text{intra},k}, \psi_{\text{inter},k}, \bar{\mathbf{C}}_k\}_{k=1}^K$,

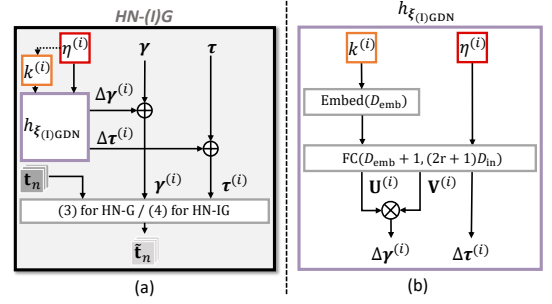


Fig. 5. (a) Adaptation process for (I)GDN parameters of HN-(I)G layer. The dashed arrow from $\eta^{(i)}$ to $k^{(i)}$ indicates that $k^{(i)}$ is determined according to $\eta^{(i)}$. (b) Network architecture of hypernetwork $h_{\xi_{(I)GDN}}$ in HN-(I)G layer.

where, for a given block with modulation order $k^{(i)}$ corresponding to block-wise SNR $\eta^{(i)}$, only the associated parameters, i.e., $\{\psi_{\text{intra},k^{(i)}}, \psi_{\text{inter},k^{(i)}}, \bar{\mathbf{C}}_{k^{(i)}}\}$, are activated to generate an adaptive codebook $\mathbf{C}^{(i)} = \mathcal{C}_{\Psi}(\eta^{(i)})$ for the i -th block. In fact, this design is analogous to the design principle of MLP-Mixer architectures [22], where feature vector processing is decomposed into intra-feature and inter-feature transformations. It is realized by lightweight MLPs, which effectively achieve the global expressivity comparable to much more computationally complex attention mechanisms of transformers. In a similar manner, our DCG network leverages base codebooks in conjunction with compact MLP layers to produce codebooks specialized for $\eta^{(i)}$ and $k^{(i)}$, achieving fine-grained adaptation with high efficiency in both parameterization and computation.

C. Hypernetwork-based Normalization Layer

Normalization layers significantly facilitate the training of NN models and enhance their performance by stabilizing the statistics of an output tensor from each NN layer. As established in uJSCC [14], the adaptability of VQ-JSCC networks that supply different modulation orders and codebooks is significantly improved through separate switchable normalization layers for each modulation order. However, since it is required to adopt codebooks according to the continuous-valued SNR input within a given modulation order, this approach is ill-suited for our framework, leading to prohibitive parameter overhead if naively extended.

To overcome this limitation, we adopt a hypernetwork³-based approach inspired by adaptive instance normalization

³A hypernetwork is a small auxiliary network that produces the parameters of another network based on conditioning variables.

(AdaIN) [23], where normalization parameters are dynamically generated from conditioning variables. Specifically, instead of storing excessive sets of normalization parameters, we employ a lightweight hypernetwork that produces normalization parameters conditioned on the block-wise SNR $\eta^{(i)}$ and the corresponding modulation order index $k^{(i)}$ determined by (1). This principle is applied to adapt the (I)GDN layers in the JSCC encoder–decoder in Section III-A and the LN layers for the DCG network in Section III-B), as detailed below.

1) *Hypernetwork-based (I)GDN Layer*: The standard GDN operation in (8) relies on fixed trainable parameters: a bias vector τ and a coefficient matrix γ . To condition the GDN operation on $\eta^{(i)}$, we introduce a hypernetwork that generates additive offsets $\Delta\tau^{(i)} \in \mathbb{R}^{D_{\text{in}}}$ and $\Delta\gamma^{(i)} \in \mathbb{R}^{D_{\text{in}} \times D_{\text{in}}}$ based on $\eta^{(i)}$ and $k^{(i)}$. As illustrated in Fig. 5(a), the adapted parameters for the i -th block are $\tau^{(i)} = \tau + \Delta\tau^{(i)}$, $\gamma^{(i)} = \gamma + \Delta\gamma^{(i)}$. The offsets are generated by a hypernetwork $h_{\xi_{\text{GDN}}}$, which embeds $k^{(i)}$, concatenates it with $\eta^{(i)}$, and maps the result through a single fully connected layer.

However, directly generating $\Delta\gamma^{(i)}$ requires an output size of $\mathcal{O}(D_{\text{in}}^2)$, resulting in an excessive number of parameters in $h_{\xi_{\text{GDN}}}$, which can be comparable to the entire JSCC model. To mitigate this overhead, we adopt the low-rank adaptation (LoRA) method [24] and decompose $\Delta\gamma^{(i)} = \mathbf{U}^{(i)}\mathbf{V}^{(i)}$, where $\mathbf{U}^{(i)} \in \mathbb{R}^{D_{\text{in}} \times r}$ and $\mathbf{V}^{(i)} \in \mathbb{R}^{r \times D_{\text{in}}}$ with $r \ll D_{\text{in}}$. Accordingly, as shown in Fig. 5(b), the hypernetwork outputs

$$\mathbf{U}^{(i)}, \mathbf{V}^{(i)}, \Delta\tau^{(i)} = h_{\xi_{\text{GDN}}}(\eta^{(i)}, k^{(i)}). \quad (15)$$

This reduces the hypernetwork parameter from $\mathcal{O}(D_{\text{in}}^2)$ to $\mathcal{O}(D_{\text{in}}r)$. We refer to this adaptive normalization layer as the HN-G layer. The same procedure is applied to IGDN layers using a separate hypernetwork $h_{\xi_{\text{IGDN}}}$, which is referred to as the HN-IG layer.

Remark 3 (HN-(I)G layers in \mathcal{F}_{Θ} and \mathcal{G}_{Φ}). *These layers replace the (I)GDN layers in the JSCC encoder–decoder and adaptively normalize the feature vector statistics between NN layers according to the channel conditions. In particular, similar to how the slimmable operation is applied to the GDN layer, HN-G layer can also be integrated with the slimmable operations in Section III-A. The full-dimensional adapted parameters $\tau^{(i)} \in \mathbb{R}^{D_{\text{max}}}$ and $\gamma^{(i)} \in \mathbb{R}^{D_{\text{max}} \times D_{\text{max}}}$ are computed first. Then, to process a tensor with a target dimension D_{target} , only the leading sub-vector $[\tau^{(i)}]_{:D_{\text{target}}}$ and sub-matrix $[\gamma^{(i)}]_{:D_{\text{target}}:D_{\text{target}}}$ are used to perform the normalization.*

2) *Hypernetwork-based LN Layer*: Notably, the proposed hypernetwork-based adaptation is generally applicable to normalization layers with trainable parameters and is therefore also applied to LN layers in the DCG network. The standard LN operation, which incorporates normalization by the mean μ_n and variance σ_n^2 of \mathbf{t}_n , is given by

$$\tilde{t}_{n,d,p} = \frac{t_{n,d,p} - \mu_n}{\sqrt{\sigma_n^2}} \cdot \alpha_d + \beta_d, \quad (16)$$

where $\alpha, \beta \in \mathbb{R}^{D_{\text{in}}}$ are trainable scale and bias vectors. Similar to the HN-(I)G layer, a hypernetwork $h_{\xi_{\text{LN}}}$, which shares the same structure as $h_{\xi_{\text{GDN}}}$, generates offset vectors

$$\Delta\alpha^{(i)}, \Delta\beta^{(i)} = h_{\xi_{\text{LN}}}(\eta^{(i)}, k^{(i)}), \quad (17)$$

which are added as $\alpha^{(i)} = \alpha + \Delta\alpha^{(i)}$ and $\beta^{(i)} = \beta + \Delta\beta^{(i)}$. Here, since LN uses only D_{in} -dimensional tensor channel-wise scale vectors, the LoRA approach is not required. We refer to this LN-based design as the HN-L layer.

Remark 4 (HN-L layer in \mathcal{C}_{Ψ}). *This layer replaces the LN layer in $\text{MLP}_{\psi_{k^{(i)}}}$ of the DCG network and adaptively normalizes intra- and inter-codeword distributions according to instantaneous channel conditions.*

IV. TRAINING STRATEGY

This section describes the overall training procedure of the proposed euJSCC framework. Directly training the model under block fading conditions substantially increases optimization difficulty and often leads to unstable convergence. To mitigate this issue, we adopt a curriculum learning strategy consisting of two stages. In the first stage, the model is pretrained without the inner encoder–decoder modules, i.e., only the outer encoder–decoder and the codebook-related modules are trained. In the second stage, the inner modules are optimized while finetuning the pretrained parameters.

A. First Stage: Training under AWGN Channels

Since we set $\mathbb{E}[|h^{(i)}|^2] = 1$, the average SNR used in the outer encoder–decoder, $\eta^{(\text{a})}$, reduces to P/σ^2 , which remains constant across all coherence blocks. Moreover, since the codebook generator also relies on $\eta^{(\text{a})}$, i.e., $|h^{(i)}| = 1$ for $i \in [1:U]$, the first stage can effectively be regarded as training over a static AWGN channel. In this setting, the communication process of the modified euJSCC framework is represented in **Algorithm 2**. The transmission can be treated as a single coherence block, i.e., $U = 1$ and $T = N$, allowing the block-wise operations in **Algorithm 1** to be omitted. Accordingly, all variables $\mathbf{C}^{(\text{a})}$, $\mathbf{z}^{(\text{a})}$, $\mathbf{s}^{(\text{a})}$, $\tilde{\mathbf{s}}^{(\text{a})}$, and $\hat{\mathbf{z}}^{(\text{a})}$ are defined with respect to $\eta^{(\text{a})}$ instead of $\eta^{(i)}$.

Specifically, the euJSCC process under the AWGN channel proceeds as follows. The outer encoder $f_{\theta_{\text{outer}}}$ encodes \mathbf{X} into \mathbf{Y}_{mid} conditioned on $\eta^{(\text{a})}$, which is then quantized using the generated codebook $\mathbf{C}^{(\text{a})} = \mathcal{C}_{\Psi}(\eta^{(\text{a})})$. The quantized indices $\mathbf{z}^{(\text{a})}$ are modulated into $\mathbf{s}^{(\text{a})}$ and transmitted through the static AWGN channel with $\eta^{(\text{a})}$. The received signal $\tilde{\mathbf{s}}^{(\text{a})}$ is demodulated and dequantized to obtain $\hat{\mathbf{z}}^{(\text{a})}$ and the corresponding $\hat{\mathbf{Y}}_{\text{mid}}$ using $\mathbf{C}^{(\text{a})}$. Finally, the outer decoder $g_{\phi_{\text{outer}}}$ reconstructs $\hat{\mathbf{X}}$ from $\hat{\mathbf{Y}}_{\text{mid}}$ conditioned on $\eta^{(\text{a})}$.

In the first training phase, only the outer encoder–decoder pair $(f_{\theta_{\text{outer}}}, g_{\phi_{\text{outer}}})$ and the codebook generator \mathcal{C}_{Ψ} are trained, while the inner encoder–decoder pair $(f_{\theta_{\text{inner}}}, g_{\phi_{\text{inner}}})$ is excluded. Accordingly, the trainable parameter set is $\varphi^{(\text{i})} = \{\theta_{\text{outer}}, \phi_{\text{outer}}, \Psi\}$. The overall procedure is summarized in **Phase 1** of **Algorithm 3**.

To optimize the model across the full SNR range, the training SNR interval is divided into J subranges, defined by the boundaries $\mathbf{r}^{(\text{i})} = [r_0^{(\text{i})}, \dots, r_J^{(\text{i})}]$. In each training iteration, a continuous-valued $\eta^{(\text{a})}$ is randomly sampled from one of these subranges according to $\eta^{(\text{a})} \sim \text{Unif}[r_{j-1}^{(\text{i})}, r_j^{(\text{i})}]$, i.e., $r_{j-1}^{(\text{i})} \leq \eta^{(\text{a})} < r_j^{(\text{i})}$, for $j \in [1:J]$. The corresponding modulation order m_k is then determined based on the modulation

Algorithm 2 Modified euJSCC for AWGN Channels

- 1: **Input:** Source image \mathbf{X} , average SNR $\eta^{(a)}$, corresponding modulation order $m_{k^{(a)}}$, outer encoder-decoder $(f_{\theta_{\text{outer}}}, g_{\theta_{\text{outer}}})$, DCG network \mathcal{C}_{Ψ}
- 2: Encode \mathbf{X} into \mathbf{Y}_{mid} with η via $f_{\theta_{\text{outer}}}$
- 3: Generate $\mathbf{C}^{(a)}$ from $\eta^{(a)}$ via \mathcal{C}_{Ψ}
- 4: Quantize \mathbf{Y}_{mid} into $\mathbf{z}^{(a)}$ using $\mathbf{C}^{(a)}$
- 5: Modulate $\mathbf{z}^{(a)}$ into $\mathbf{s}^{(a)}$ via $m_{k^{(a)}}$ -ary modulation
- 6: Transmit $\mathbf{s}^{(a)}$ through AWGN channel with $\eta^{(a)}$
- 7: Demodulate $\tilde{\mathbf{s}}^{(a)}$ into $\hat{\mathbf{z}}^{(a)}$ via $m_{k^{(a)}}$ -ary modulation
- 8: Dequantize $\hat{\mathbf{z}}^{(a)}$ into $\hat{\mathbf{Y}}_{\text{mid}}$ using $\mathbf{C}^{(a)}$
- 9: Reconstruct $\hat{\mathbf{X}}$ from $\hat{\mathbf{Y}}_{\text{mid}}$ with $\eta^{(a)}$ via $g_{\theta_{\text{outer}}}$
- 10: **Output:** $\hat{\mathbf{X}}$

Algorithm 3 euJSCC Training Algorithm

1: **Input:** Training dataset \mathcal{D} , modulation set $\{m_k\}_{k=1}^K$, training SNR boundary $\mathbf{r}^{(i)} = [r_0^{(i)}, \dots, r_J^{(i)}]$, $\mathbf{r}^{(ii)} = [r_0^{(ii)}, \dots, r_J^{(ii)}]$, modulation selection SNR boundary $\mathbf{b} = [b_1, \dots, b_{K-1}]$, loss weights $\{\lambda_j^{(i)}\}_{j=1}^J$, $\{\lambda_j^{(ii)}\}_{j=1}^J$, minimum and maximum coherence block length (T_{\min} , T_{\max})

Phase 1: Training under AWGN channels

```

2: Initialize  $\varphi^{(i)} = \{\theta_{\text{outer}}, \phi_{\text{outer}}, \Psi\}$ 
3: while Stopping criterion is not met do
4:   Sample  $\mathbf{X} \sim \mathcal{D}$ ;  $\mathcal{L}_{\text{total}} \leftarrow 0$  // mini-batch
5:   for  $j \leftarrow 1$  to  $J$  do
6:     Sample  $\eta^{(a)} \sim \text{Unif}[r_{j-1}^{(i)}, r_j^{(i)})$ 
7:     Choose  $m_{k^{(a)}}$  by  $\eta^{(a)}$  and  $\mathbf{b}$  with (1)
8:     Compute  $\mathcal{L}_j$  as in (7) via Algorithm 2
9:      $\mathcal{L}_{\text{total}} \leftarrow \mathcal{L}_{\text{total}} + \lambda_j^{(i)} \mathcal{L}_j$ 
10:    Update  $\varphi^{(i)}$  with  $\mathcal{L}_{\text{total}}$ 
11: Output:  $\varphi^{(i)*} = \{\theta_{\text{outer}}^*, \phi_{\text{outer}}^*, \Psi^*\}$ 

```

Phase 2: Training under block fading channels

```

12: Initialize  $\{\theta_{\text{inner}}, \phi_{\text{inner}}\}$ 
13: Define  $\varphi^{(ii)} = \varphi^{(i)*} \cup \{\theta_{\text{inner}}, \phi_{\text{inner}}\}$ 
14: while Stopping criterion is not met do
15:   Sample  $\mathbf{X} \sim \mathcal{D}$ ;  $\mathcal{L}_{\text{total}} \leftarrow 0$  // mini-batch
16:   for  $j \leftarrow 1$  to  $J$  do
17:     Sample  $\eta^{(a)} \sim \text{Unif}[r_{j-1}^{(ii)}, r_j^{(ii)})$ 
18:     Sample  $T \sim \text{Unif}[T_{\min} : T_{\max}]$ 
19:     Sample  $\{h^{(i)}\}_{i=1}^U \sim \mathcal{CN}(0, 1)$ 
20:     Calculate  $\{\eta^{(i)}\}_{i=1}^U$ 
21:     Choose  $\{m_{k^{(i)}}\}_{i=1}^U$  by  $\{\eta^{(i)}\}_{i=1}^U$  and  $\mathbf{b}$  with (1)
22:     Compute  $\mathcal{L}_j$  as in (7) via Algorithm 1
23:      $\mathcal{L}_{\text{total}} \leftarrow \mathcal{L}_{\text{total}} + \lambda_j^{(ii)} \mathcal{L}_j$ 
24:   Update  $\varphi^{(ii)}$  with  $\mathcal{L}_{\text{total}}$ 
25: Output:  $\varphi^{(ii)*} = \{\theta_{\text{outer}}^*, \phi_{\text{outer}}^*, \Psi^*, \theta_{\text{inner}}^*, \phi_{\text{inner}}^*\}$ 

```

thresholds b using (1). For each sampled $\eta^{(a)}$ in the subrange, the model performs a forward pass following **Algorithm 2** to compute the loss \mathcal{L}_j as in (7). The total loss for the first phase is obtained by aggregating the individual subrange losses: $\mathcal{L}_{\text{total}} = \sum_{i=1}^J \lambda_j^{(i)} \mathcal{L}_j$, where $\lambda_j^{(i)}$ is a weighting

factor that balances the contribution of each SNR subrange by compensating for differences in loss scale. Finally, the parameter set $\varphi^{(i)}$ is updated using the Adam optimizer based on the aggregated loss $\mathcal{L}_{\text{total}}$. Training proceeds until the termination conditions outlined in Section V are met.

B. Second Stage: Training under Block Fading Channels

In the second training phase, the inner encoder-decoder pair ($f_{\theta_{\text{inner}}}$ and $g_{\phi_{\text{inner}}}$) is activated, and jointly trained with the optimized parameters $\varphi^{(i)*}$ from the first phase. The trainable parameter set for this phase is thus initialized as $\varphi^{(ii)} = \varphi^{(i)*} \cup \{\theta_{\text{inner}}, \phi_{\text{inner}}\}$. The whole training process for the second phase is summarized in **Phase 2** of **Algorithm 3**.

Unlike the AWGN scenario, the block-wise SNR varies across coherence blocks, and each block i is explicitly considered. At each iteration, given the training SNR boundary $\mathbf{r}^{(ii)} = [r_0^{(ii)}, \dots, r_J^{(ii)}]$ for the second phase, a continuous-valued average SNR $\eta^{(a)}$ is randomly sampled from the continuous uniform distribution $\text{Unif}[r_{j-1}^{(ii)}, r_j^{(ii)}]$, i.e., $r_{j-1}^{(ii)} \leq \eta < r_j^{(ii)}$, for $j \in [1:J]$. For each j , to allow a single euJSCC model to support variable coherence block lengths, the block size T is randomly drawn from the discrete uniform distribution $\text{Unif}[T_{\min}:T_{\max}]$, i.e., $T \in [T_{\min}:T_{\max}]$. Subsequently, for each block $i \in [1:U]$, the channel coefficient is sampled as $h^{(i)} \sim \mathcal{CN}(0, 1)$ and the corresponding block-wise SNR $\eta^{(i)}$ is calculated. The modulation orders $m_{k^{(i)}}$ and $m_{k^{(a)}}$ are determined by $\eta^{(i)}$, $\eta^{(a)}$, and the threshold set \mathbf{b} .

The loss \mathcal{L}_j for each SNR subrange is computed according to (7) following **Algorithm 1**. The total loss for the second phase is obtained by aggregating these subrange losses: $\mathcal{L}_{\text{total}} = \sum_{j=1}^J \lambda_j^{(\text{ii})} \mathcal{L}_j$, where $\lambda_j^{(\text{ii})}$ balances the contributions of different SNR subranges. Finally, the parameter set $\varphi^{(\text{ii})} = \{f_{\theta_{\text{outer}}}, g_{\phi_{\text{outer}}}, \Psi, f_{\theta_{\text{inner}}}, g_{\phi_{\text{inner}}}\}$ is iteratively updated using the Adam optimizer. Training continues until the stopping criterion specified in Section V is satisfied.

V. EXPERIMENTAL RESULTS

The proposed euJSCC model is trained on the DIV2K training dataset, where the original images have 2K resolution. During training, the images are randomly cropped into patches of size 256×256 . The dataset is divided into training and validation subsets in a 9:1 ratio, and validation is performed after every epoch. Training is terminated if no improvement is observed over 100 consecutive validations. Performance is evaluated on three datasets: the DIV2K test dataset, the CLIC2021 test set, which consists of high-resolution images of approximately 2K resolution, and the Kodak dataset with image size 512×768 . The channel bandwidth ratio (CBR), defined as the ratio between the number of transmitted channel symbols and the dimensionality of the source data, is set to $\frac{N}{CHW} = \frac{1}{48}$. The network architectures of the encoder-decoder in euJSCC are summarized in Table I. The notations used in the tables are defined as follows:

- $\text{Conv2D}(c_{\text{in}}, c_{\text{out}}, f, s, p)$ and $\text{T-Conv2D}(c_{\text{in}}, c_{\text{out}}, f, s, p)$: 2D convolutional and transposed convolutional layers, parameterized by input tensor channel dimensions c_{in} ,

TABLE I
NN STRUCTURE OF THE EUJSCC ENCODER AND DECODER (THE NOTATION $\{\cdot\}_{k=1}^K$ DENOTES K PARALLEL LAYERS.)

Module	Layers	Output size
Outer encoder	Conv2D($C, c_1, 4, 2, 1$) + HN-G(c_1) + PReLU	$c_1 \times H/2 \times W/2$
	Conv2D($c_1, c_2, 4, 2, 1$) + HN-G(c_2) + PReLU	$c_2 \times H/4 \times W/4$
	Res(c_2) + PReLU	$c_2 \times H/4 \times W/4$
	Conv2D($c_2, c_1, 5, 1, 2$) + HN-G(c_1) + PReLU	$c_1 \times H/4 \times W/4$
	Res(c_1) + PReLU	$c_1 \times H/4 \times W/4$
	Conv2D($c_1, D_K, 5, 1, 2$) + HN-G(D_K) + Reshape	$D_{k^{(a)}} \times HW/16$
Inner encoder	$\{\text{Conv1D}(D_k, D_K, 5, 1, 2)\}_{k=1}^K + \{\text{HN-G}(D_k)\}_{k=1}^K$	$D_{k^{(i)}} \times HW/16$
Inner decoder	$\{\text{Conv1D}(D_k, D_K, 5, 1, 2)\}_{k=1}^K + \{\text{HN-IG}(D_k)\}_{k=1}^K$	$D_{k^{(a)}} \times HW/16$
Outer decoder	Reshape + T-Conv2D($D_K, c_1, 5, 1, 2$) + HN-IG(c_1) + PReLU	$c_1 \times H/4 \times W/4$
	T-Res(c_1) + PReLU	$c_1 \times H/4 \times W/4$
	T-Conv2D($c_1, c_2, 5, 1, 2$) + HN-IG(c_2) + PReLU	$c_2 \times H/4 \times W/4$
	T-Res(c_2) + PReLU	$c_2 \times H/4 \times W/4$
	T-Conv2D($c_2, c_1, 4, 2, 1$) + HN-IG(c_1) + PReLU	$c_1 \times H/2 \times W/2$
	T-Conv2D($c_1, C, 4, 2, 1$) + HN-IG(C) + Reshape	$C \times H \times W$
Res(c)	Conv2D($c, c, 3, 1, 1$) + HN-G(c) + PReLU	$c \times h \times w$
	Conv2D($c, c, 1, 1, 0$) + HN-G(c)	$c \times h \times w$
T-Res(c)	T-Conv2D($c, c, 1, 1, 0$) + HN-IG(c) + PReLU	$c \times h \times w$
	T-Conv2D($c, c, 3, 1, 1$) + HN-IG(c)	$c \times h \times w$

output channel dimensions c_{out} , kernel size f , stride s , and padding p .

- Conv1D($c_{\text{in}}, c_{\text{out}}, f, s, p$): 1D convolutional layers, defined in the same manner as in the 2D case.
- Res(c) and T-Res(c): Residual and transposed residual blocks with input tensor channel dimensions c , each preserving the spatial dimension of the input.
- Reshape: A tensor reshaping operation, used to reorder or merge/split dimensions.
- PReLU and Tanh: Activation functions, corresponding to the parameterized rectified linear unit and the hyperbolic tangent, respectively.
- HN-G(c) and HN-IG(c): The proposed hypernetwork-based GDN and inverse GDN layers with input tensor channel dimensions c .

To validate the enhanced channel adaptability of euJSCC, we conduct experiments under both block fading and AWGN channels. The models, including the proposed euJSCC, employed for the comparison are listed below:

- **euJSCC-A:** This version of euJSCC is trained only in the first phase of **Algorithm 3** and evaluated under AWGN channels. Here, the inner encoder-decoder module is not included.
- **euJSCC-B:** The full euJSCC model is trained through both phases of **Algorithm 3** and evaluated under block fading channels.
- **euJSCC-S:** It consists of independently trained euJSCC-A models for each SNR interval $[b_{k-1}, b_k)$ and modulation order m_k , serving as an upper bound for performance and a reference for parameter efficiency.
- **uJSCC-A:** The model follows the uJSCC framework in [14]. Each convolutional layer is followed by a switchable (inverse) GDN layer that internally contains K (inverse) GDN layers and employs modulation-specific codebooks, both of which are activated according to the input index $k^{(a)}$. All training hyperparameters match those of euJSCC.
- **uJSCC-B:** Since the original uJSCC is not designed to

operate under block fading channels, this model extends uJSCC by enabling block-wise processing. Specifically, an inner encoder and decoder with the same structure as those in euJSCC-B are inserted between the uJSCC encoder and decoder, while the normalization layers are implemented as switchable (inverse) GDN layers. These normalization layers include a total of K^2 (inverse) GDN layers, each activated according to the combination of $(k^{(a)}, k^{(i)})$.

- **MDJCM-A:** It is the MDJCM model proposed in [10] is a channel-adaptive, SQ-JSCC model that performs SNR- and modulation-conditioned adaptation on the values of feature vectors, along with entropy-based adjustment of feature vector lengths. The model is trained following the three-phase training procedure under AWGN channels as described in [10]. The Swin Transformer backbone in the analysis and synthesis transform networks is replaced with a CNN-based architecture, so that performance differences between MDJCM and euJSCC are not attributed to backbone architectural choices and a fair comparison is ensured.
- **MDJCM-B:** This model extends MDJCM-A to block fading channels. The original MDJCM assumes a fixed SNR for the entire transmission of feature vectors. Moreover, due to its entropy-based feature vector-length adjustment, the resulting feature vectors have varying lengths, making it difficult to apply the inner encoder-decoder as in euJSCC. To adapt it to the block fading scenario, the average SNR and its corresponding modulation order are fed to the adaptation modules of the encoder and decoder, while the modulation order used for each coherence block is chosen dynamically according to the block-wise SNR.

Hyperparameters for training are as follows: the learning rate is set to 10^{-4} , and the batch size is 4. The system supports $K = 5$ modulation orders, namely BPSK, 4QAM, 16QAM, 64QAM, and 256QAM, where the modulation order is $m_k \in \{2, 4, 16, 64, 256\}$ and the corresponding feature

TABLE II
HYPERPARAMETERS FOR TRAINING EUJSCC ($\mathbf{r}^{(i)}$, $\mathbf{r}^{(ii)}$, \mathbf{b} , $\{\lambda_j^{(i)}\}$, $\{\lambda_j^{(ii)}\}$, AND α_k ARE LISTED SEQUENTIALLY IN INCREASING ORDER OF j AND k .)

Hyperparameters	Values
J	5
T_{\min}, T_{\max}	64, 1024
$\mathbf{r}^{(i)} = [r_0^{(i)}, \dots, r_J^{(i)}]$	-5, 5, 12, 20, 26, 35
$\mathbf{r}^{(ii)} = [r_0^{(ii)}, \dots, r_J^{(ii)}]$	3, 8, 13, 18, 23, 27
$\mathbf{b} = [b_1, \dots, b_{K-1}]$	5, 12, 20, 26
$\{\lambda_j^{(i)}\}_{j=1}^J$	1, 2, 3, 6, 12
$\{\lambda_j^{(ii)}\}_{j=1}^J$	1, 2, 3, 6, 12
$\{\alpha_k\}_{k=1}^K$	3, 2, 1, 0.7, 0.5

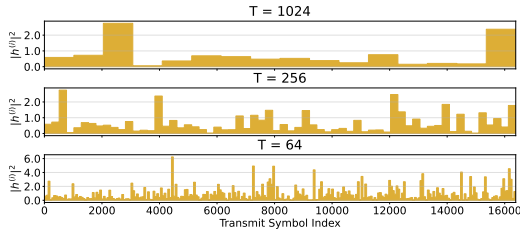


Fig. 6. An illustration of channel gain realizations $|h^{(i)}|^2$ under the block fading channel for different coherent block length T .

vector channel dimension is $D_k \in \{4, 8, 16, 24, 32\}$, empirically selected to improve feature vector expressiveness while limiting quantization distortion [14]. For all the HN-(I)G layers, the low rank r is set to 4. The remaining hyperparameters are summarized in Table II. Following [25], we regard each feature vector as a block in the conventional communication system, and \mathbf{b} is set to target a symbol error rate (SER) of approximately 0.1, in line with the setting adopted in [14]. We evaluate the task performance of image transmission using peak signal-to-noise ratio (PSNR) and multi-scale structural similarity (MS-SSIM). For improved interpretability, MS-SSIM is reported in dB scale using the transformation $\text{MS-SSIM}(\text{dB}) = -10 \log(1 - \text{MS-SSIM})$.

A. Performance Analysis under Block Fading Channels

We first evaluate the performance under block fading channels, where the channel gain remains constant for T symbols. Fig. 6 provides illustrative examples of the channel gain realizations $|h^{(i)}|^2$ for the different T values used in our experiments. To mitigate the performance fluctuations caused by specific channel gain realizations, we perform 50 independent evaluations with different realizations for each input image and report the total averaged results over the test dataset. For blocks where $|h^{(i)}|^2 \approx 0$, resulting in $\eta^{(i)} < -5$ dB, even the most robust modulation scheme yields severely distorted received codewords. As a result, in such cases, we skip transmission and instead resample the channel coefficients for both the training and evaluation.

Fig. 7 presents the PSNR and MS-SSIM results of euJSCC-B, uJSCC-B, and MDJCM-B under block fading channels. Across all datasets and T values, euJSCC-B consistently outperforms uJSCC-B in both metrics, demonstrating the effectiveness of its fine-grained, block-wise SNR-based channel adaptation. Compared with MDJCM-B, euJSCC-B achieves comparable performance at low average SNRs below 12 dB,

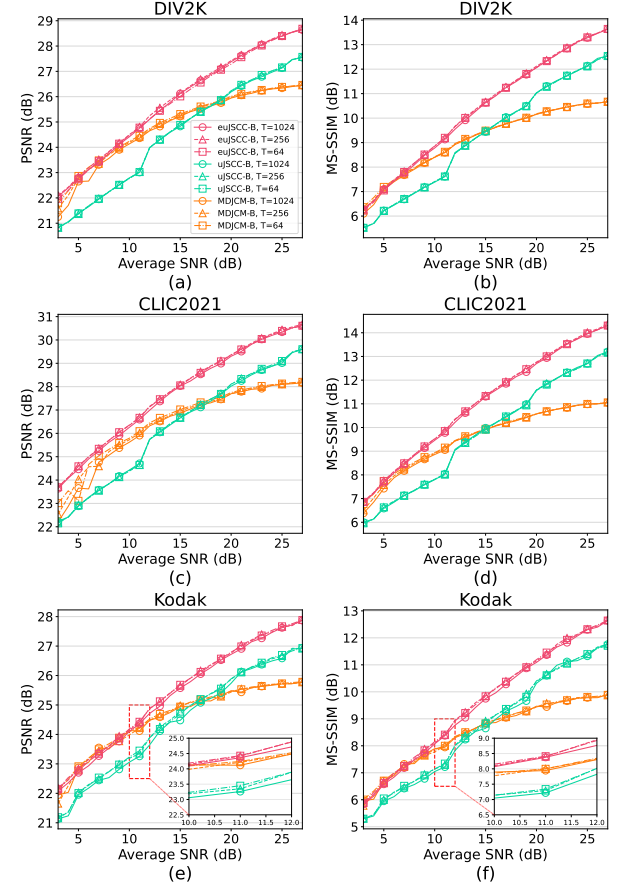


Fig. 7. Performance comparison of the proposed euJSCC-B against baselines under block fading channels with three test datasets of DIV2K, CLIC2021, and Kodak.

where MDJCM benefits from entropy-based feature-length adaptation and the gain of VQ over SQ becomes marginal due to small codebooks. However, as the average SNR increases, MDJCM-B quickly saturates, whereas euJSCC-B continues to improve through both the enhanced channel adaptability from inner encoder/decoder refinement with block-wise SNR and the use of higher-order modulations and larger codebooks. In addition, both PSNR and MS-SSIM slightly increase as T decreases across all datasets, particularly for the Kodak dataset in Figs. 7(e) and (f), since larger T increases the likelihood that adjacent feature vectors are simultaneously affected by deep fades, causing local information loss during decoding.

B. Parameter Efficiency

As shown in Table III, the parameters associated with the channel-adaptive modules, i.e., the hypernetworks $h_{\xi^{(1)}_{\text{GDN}}}$ in HN-G layers, and the DCG network \mathcal{C}_{Ψ} , account for only about 3.7% of the total parameters in euJSCC. Notably, if $h_{\xi^{(1)}_{\text{GDN}}}$ directly generates the offset terms $\Delta\gamma^{(i)}$ and $\Delta\tau^{(i)}$ without employing the LoRA approach, it requires more than about 28 \times parameters compared to the LoRA-based implementation. Furthermore, the inner encoder-decoder is composed of a single set of parallel (transposed) convolutional layers and HN-(I)G layers that support slimmable operation, occupying only about 0.5% of the total parameters. These results demonstrate that the proposed adaptive design achieves fine-grained channel adaptability with minimal memory overhead.

TABLE III

NUMBER OF PARAMETERS ACROSS MODELS (FOR EUJSCC, THE PORTION OF THE PARAMETERS IN INDIVIDUAL LAYERS COMPARED TO THE FULL EUJSCC MODEL IS REPRESENTED WITH A PERCENTAGE.)

Model	# of Params.	Portion (%)
euJSCC-A	9,711,790	—
HN-(I)G	1,117,902	8.7
$h_{\xi_{(I)GDN}}$ for HN-(I)G	197,312	2.0
$(h_{\xi_{(I)GDN}})$ w/o LoRA	5,532,936	—
\mathcal{C}_{Ψ}	158,429	1.7
euJSCC-B	9,759,356	—
$f_{\theta_{inner}}, g_{\phi_{inner}}$	47,566	0.5
uJSCC-A [14]	13,053,022	—
uJSCC-B [14]	13,100,112	—
MDJCM-A, MDJCM-B [10]	11,006,018	—
euJSCC-S	46,977,851	—

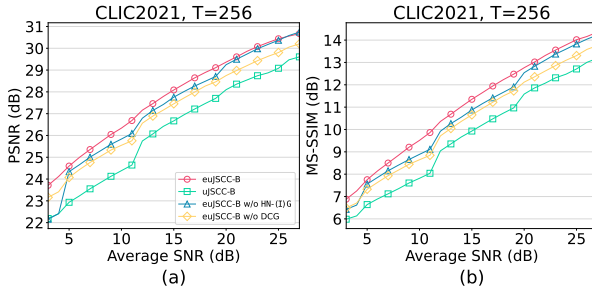


Fig. 8. Performance comparison of euJSCC-B against its variants and uJSCC-B in terms of (a) PSNR and (b) MS-SSIM for CLIC2021 dataset with $T = 256$.

C. Component-Wise Analysis

To systematically evaluate the efficacy of our proposed components, we conduct an ablation study on block fading channels. Specifically, we extend the comparison between uJSCC-B and euJSCC-B by introducing two baselines to disentangle the individual contributions of the proposed modules for adaptation. The baselines are detailed as follows:

- (i) **euJSCC-B w/o HN-(I)G:** This variant of euJSCC-B incorporates \mathcal{C}_{Ψ} but replaces the HN-(I)G layers in \mathcal{F}_{Θ} and \mathcal{G}_{Φ} with switchable (inverse) GDN layers, each activated according to the combination of $(k^{(a)}, k^{(i)})$.
- (ii) **euJSCC-B w/o DCG:** The euJSCC-B model is equipped with HN-(I)G layers in \mathcal{F}_{Θ} and \mathcal{G}_{Φ} , but uses static, modulation-specific codebooks instead of dynamically generated ones from \mathcal{C}_{Ψ} .

As shown in Fig. 8, a clear performance hierarchy is observed among the four models. The superior performance of euJSCC-B w/o HN-(I)G over euJSCC-B w/o DCG highlights the importance of codebook adaptation in VQ-JSCC, as static modulation-specific codebooks suppress the benefits of SNR-aware feature encoding and decoding due to quantization with fixed codewords. In contrast, dynamic codebook adaptation better matches instantaneous channel conditions, improving stronger robustness. Furthermore, uJSCC-B and euJSCC-B w/o HN-(I)G, which rely on switchable (inverse) GDN layers, exhibit abrupt PSNR and MS-SSIM variations near modulation-switching SNR thresholds (e.g., 5, 12, and 20 dB). They show insufficient feature vector refinement across SNR ranges and it is confirmed that the proposed HN-(I)G layer enables effective adaptation than switchable normalization. Finally, since euJSCC-B achieves the highest

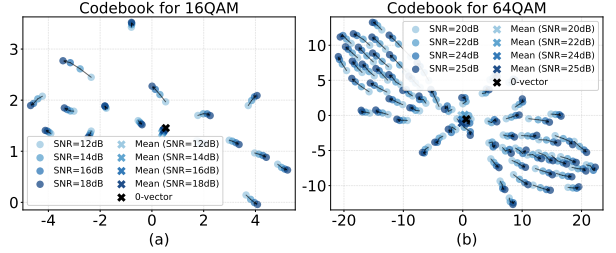


Fig. 9. A t-SNE visualization of the codebooks generated from the DCG network for (a) 16-QAM and (b) 64-QAM for different input SNRs. Colored and black cross markers represent the t-SNE visualization of the mean codewords for each SNR and the reference 0-vector, respectively. The trajectory for each codeword indicates how the codeword shifts with varying SNRs.

PSNR and MS-SSIM across all SNR levels, it can be inferred that jointly adjusting the encoder, decoder, and codebook for fine-grained SNR conditions is essential and compelling for achieving robust semantic communication under diverse channel environments.

D. Codebook Analysis

To examine how the euJSCC-B codebooks are generated by \mathcal{C}_{Ψ} under different modulation orders and input SNRs, we visualize their distributions using t-distributed stochastic neighboring embedding (t-SNE), as shown in Figs. 9(a) and (b) for 16QAM and 64QAM, respectively. The t-SNE method projects high-dimensional codewords into a two-dimensional space while approximately preserving pairwise similarities, where spatial proximity reflects codeword similarity and the overall spread indicates codebook expressiveness. For both modulations, the mean codeword locations remain similar across SNRs. As the SNR decreases (from deeper to lighter blue), the codewords cluster more tightly around the mean, indicating reduced inter-codeword separation. In contrast, at higher SNRs (from lighter to deeper blue), the codewords become more dispersed, exhibiting larger separation and wider spatial coverage. This trend suggests that, at low SNRs, the model favors more similar codewords to enhance robustness against channel noise albeit at the cost of reduced expressiveness of the codebook. On the other hand, at high SNRs, it increases codeword diversity to improve representational expressiveness. These results confirm that euJSCC dynamically generates codebooks that effectively balance robustness and expressiveness according to instantaneous channel conditions.

E. Performance Analysis under AWGN Channels

Under AWGN channels, the PSNR and MS-SSIM results versus average SNR are shown in Fig. 10. Compared with uJSCC-A, euJSCC-A consistently achieves higher performance across the entire SNR range, demonstrating strong adaptability even in static channels. Relative to MDJCM-A, euJSCC-A shows comparable performance at low SNRs and increasingly outperforms it as the SNR increases. Moreover, euJSCC-A attains performance comparable to euJSCC-S across all datasets and metrics, despite euJSCC-S having approximately 4.8 \times more parameters shown in Table III. These results demonstrate that even under static AWGN environments, fine-grained, SNR-conditioned adaptation in feature

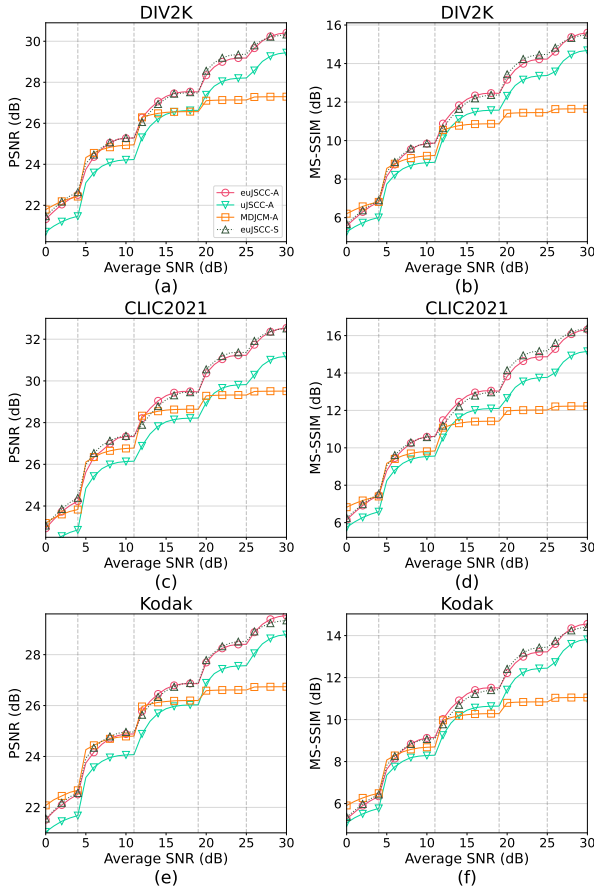


Fig. 10. Performance comparison of the proposed euJSCC against baselines under AWGN channels with test datasets of DIV2K, CLIC2021, and Kodak.

vector normalization and codebook generation significantly improves channel adaptability with high parameter efficiency.

VI. CONCLUSION

In this paper, we proposed an euJSCC framework that enables fine-grained SNR- and modulation-adaptive semantic communication within a single unified model. By integrating a hypernetwork-based normalization layer and a DCG network, euJSCC achieves continuous adaptation of the encoding/decoding and quantization processes to instantaneous channel conditions with minimal parameter overhead. Moreover, the inner-outer encoder-decoder architecture combined with a two-phase training strategy enhances robustness under block fading channels. Extensive experiments demonstrate that euJSCC consistently outperforms existing channel-adaptive digital JSCC schemes in both PSNR and MS-SSIM across a wide range of SNRs, highlighting its effectiveness and scalability for next-generation semantic communication systems.

REFERENCES

- [1] Y. Shi, Y. Zhou, D. Wen, Y. Wu, C. Jiang, and K. B. Letaief, “Task-oriented communications for 6G: Vision, principles, and technologies,” *IEEE Wireless Communications*, vol. 30, no. 3, pp. 78–85, 2023.
- [2] H. Seo, J. Park, M. Bennis, and M. Debbah, “Semantics-native communication via contextual reasoning,” *IEEE Transactions on Cognitive Communications and Networking*, vol. 9, no. 3, pp. 604–617, 2023.
- [3] H. Seo, Y. Kang, M. Bennis, and W. Choi, “Bayesian inverse contextual reasoning for heterogeneous semantics-native communication,” *IEEE Transactions on Communications*, vol. 72, no. 2, pp. 830–844, 2024.
- [4] Y. Huh, B. Kim, and W. Choi, “Feature reconstruction aided federated learning for image semantic communication,” in *IEEE Global Communications Conference (GLOBECOM)*, 2025, pp. 1–6.
- [5] —, “Federated learning with feature reconstruction for vector quantization based semantic communication,” *arXiv preprint arXiv:2508.03248*, 2025.
- [6] N. Farsad, M. Rao, and A. Goldsmith, “Deep learning for joint source-channel coding of text,” in *IEEE International Conference on Acoustics, Speech and Signal Processing (ICASSP)*, 2018, pp. 2326–2330.
- [7] G. Zhang, K. Zhou, Y. Cai, Q. Hu, and G. Yu, “Toward compatible semantic communication: A perspective on digital coding and modulation,” *IEEE Communications Magazine*, pp. 1–7, 2025.
- [8] L. Guo, W. Chen, Y. Sun, and B. Ai, “Digital-SC: Digital semantic communication with adaptive network split and learned non-linear quantization,” *IEEE Transactions on Cognitive Communications and Networking*, vol. 11, no. 4, pp. 2499–2511, 2025.
- [9] T.-Y. Tung, D. B. Kurka, M. Jankowski, and D. Gündüz, “DeepJSCC-Q: Constellation constrained deep joint source-channel coding,” *IEEE Journal on Selected Areas in Information Theory*, vol. 3, no. 4, pp. 720–731, 2022.
- [10] G. Zhang, P. Yang, Y. Cai, Q. Hu, and G. Yu, “From analog to digital: Multi-order digital joint coding-modulation for semantic communication,” *IEEE Transactions on Communications*, vol. 73, no. 6, pp. 4257–4271, 2025.
- [11] Q. Hu, G. Zhang, Z. Qin, Y. Cai, G. Yu, and G. Y. Li, “Robust semantic communications with masked VQ-VAE enabled codebook,” *IEEE Transactions on Wireless Communications*, vol. 22, no. 12, pp. 8707–8722, 2023.
- [12] S. Xie, S. Ma, M. Ding, Y. Shi, M. Tang, and Y. Wu, “Robust information bottleneck for task-oriented communication with digital modulation,” *IEEE Journal on Selected Areas in Communications*, vol. 41, no. 8, pp. 2577–2591, 2023.
- [13] W. Zheng, H. Liang, C. Dong, and X. Xu, “Deep joint source-channel coding based on feedback-driven codebook optimization,” in *IEEE Wireless Communications and Networking Conference (WCNC)*, 2025, pp. 1–6.
- [14] Y. Huh, H. Seo, and W. Choi, “Universal joint source-channel coding for modulation-agnostic semantic communication,” *IEEE Journal on Selected Areas in Communications*, vol. 43, no. 7, pp. 2560–2574, 2025.
- [15] J. Lee, H. Lee, and W. Choi, “Wireless channel adaptive DNN split inference for resource-constrained edge devices,” *IEEE Communications Letters*, vol. 27, no. 6, pp. 1520–1524, 2023.
- [16] J. Ballé, P. A. Chou, D. Minnen, S. Singh, N. Johnston, E. Agustsson, S. J. Hwang, and G. Toderici, “Nonlinear transform coding,” *IEEE Journal of Selected Topics in Signal Processing*, vol. 15, no. 2, pp. 339–353, 2020.
- [17] J. Hu, L. Shen, and G. Sun, “Squeeze-and-excitation networks,” in *IEEE Conference on Computer Vision and Pattern Recognition (CVPR)*, 2018, pp. 7132–7141.
- [18] L. Cheng, B. Henty, F. Bai, and D. D. Stancil, “Doppler spread and coherence time of rural and highway vehicle-to-vehicle channels at 5.9 GHz,” in *IEEE Global Telecommunications Conference (GTC)*, 2008, pp. 1–6.
- [19] H. Li, G. Zhang, K. Zhou, Y. Cai, and G. Yu, “Coarse-to-fine: A dual-phase channel-adaptive method for wireless image transmission,” *IEEE Transactions on Wireless Communications*, vol. 25, pp. 2607–2623, 2026.
- [20] A. Van Den Oord, O. Vinyals *et al.*, “Neural discrete representation learning,” *Advances in Neural Information Processing Systems (NeurIPS)*, vol. 30, pp. 6306–6315, 2017.
- [21] J. Yu, L. Yang, N. Xu, J. Yang, and T. Huang, “Slimmable neural networks,” *arXiv preprint arXiv:1812.08928*, 2018.
- [22] I. O. Tolstikhin, N. Houlsby, A. Kolesnikov, L. Beyer, X. Zhai, T. Unterthiner, J. Yung, A. Steiner, D. Keysers, J. Uszkoreit *et al.*, “MLP-mixer: An all-MLP architecture for vision,” *Advances in Neural Information Processing Systems (NeurIPS)*, vol. 34, pp. 24 261–24 272, 2021.
- [23] X. Huang and S. Belongie, “Arbitrary style transfer in real-time with adaptive instance normalization,” in *IEEE International Conference on Computer Vision (ICCV)*, 2017, pp. 1501–1510.
- [24] E. J. Hu, Y. Shen, P. Wallis, Z. Allen-Zhu, Y. Li, S. Wang, L. Wang, W. Chen *et al.*, “LoRA: Low-rank adaptation of large language models.” *International Conference on Learning Representations (ICLR)*, vol. 1, no. 2, p. 3, 2022.
- [25] 3GPP, “NR; Physical layer procedures for data,” 3rd Generation Partnership Project (3GPP), Technical Specification (TS) 38.214, March 2024, version 18.2.0.